β-$Cu_2V_2O_7$: A spin-$\frac{1}{2}$ honeycomb lattice system

Alexander A. Tsirlin,* Oleg Janson,† and Helge Rosner‡
Max Planck Institute for Chemical Physics of Solids, Nöthnitzer Str. 40, 01187 Dresden, Germany
(Received 2 July 2010; published 7 October 2010)

We report on band-structure calculations and a microscopic model of the low-dimensional magnet β-$Cu_2V_2O_7$. Magnetic properties of this compound can be described by a spin-$\frac{1}{2}$ anisotropic honeycomb lattice model with the averaged coupling $\bar{J}_1=60-66$ K. The low symmetry of the crystal structure leads to two inequivalent couplings J_1 and J_1' but this weak spatial anisotropy does not affect the essential physics of the honeycomb spin lattice. The structural realization of the honeycomb lattice is highly nontrivial: the leading interactions J_1 and J_1' run via double bridges of VO_4 tetrahedra between spatially separated Cu atoms while the interactions between structural nearest neighbors are negligible. The non-negligible interplane coupling $J_\perp \simeq 15$ K gives rise to the long-range magnetic ordering at $T_N \simeq 26$ K. Our model simulations improve the fit of the magnetic susceptibility data, compared to the previously assumed spin-chain models. Additionally, the simulated ordering temperature of 27 K is in remarkable agreement with the experiment. Our study evaluates β-$Cu_2V_2O_7$ as the best available experimental realization of the spin-$\frac{1}{2}$ Heisenberg model on the honeycomb lattice. We also provide an instructive comparison of different band-structure codes and computational approaches to the evaluation of exchange couplings in magnetic insulators.

DOI: 10.1103/PhysRevB.82.144416 PACS number(s): 75.30.Et, 75.10.Jm, 71.20.Ps, 75.50.Ee

I. INTRODUCTION

Quantum magnetism is one of the most exciting and promising fields for exploring exotic ground states and unusual low-temperature properties. A variety of models and lattices lead to different regimes, ranging from simple, collinear long-range order to intricate and essentially quantum ground states.[1] One of the relevant examples is the honeycomb (hexagonal) lattice that comprises a two-dimensional (2D) network of regular hexagons. The spin-$\frac{1}{2}$ Heisenberg model on the honeycomb lattice shows strong quantum fluctuations due to the low coordination number of 3.[2–4] A weak interlayer coupling stabilizes the Néel ordering with the reduced sublattice magnetization of 0.54 μ_B (compare to 1 μ_B for a classical system).[4–6] Modifications of the model dramatically change its properties. For example, frustrating next-nearest-neighbor couplings induce a spin-liquid or a valence-bond-solid ground state.[7–9] The exactly solvable Kitaev model sets a specific arrangement of Ising-type interactions on the nearest-neighbor bonds of the honeycomb lattice and also leads to a spin-liquid ground state[10] that even sustains a partial disorder.[11] Despite the diversity of intriguing theoretical predictions, experimental studies remain scarce due to the lack of appropriate model materials.

Recent studies proposed several high-spin honeycomb lattice compounds, based on Ni^{+2} (Ref. 12) and Mn^{+4} (Ref. 13). The iridates M_2IrO_3 (M=Li,Na) bear spin $\frac{1}{2}$ and likely show anisotropic exchange interactions on the honeycomb lattice.[14] In contrast, the isotropic interaction regime is typically found in Cu^{+2} or V^{+4} compounds, well to be accounted by a Heisenberg model. The apparently hexagonal arrangement of Cu atoms in $Na_3Cu_2SbO_6$ is sometimes taken as an evidence of the honeycomb-lattice magnetism.[15] However, the structural distortion and the orbital state of Cu make different bonds of the lattice inequivalent and induce one-dimensional magnetic behavior.[16] A more appropriate system could be $InCu_{2/3}V_{1/3}O_3$ but it shows intrinsic disorder due to the intermixing of spin-$\frac{1}{2}$ Cu^{+2} and nonmagnetic V^{+5} cations. Although the Cu atoms are believed to form small magnetic clusters on a honeycomb lattice,[17,18] the influence of the nonmagnetic part of this lattice is unclear and impedes the decisive comparison between experimental results and theoretical predictions. Thus, structurally ordered and well-characterized spin-$\frac{1}{2}$ honeycomb-lattice materials with essentially isotropic, Heisenberg exchange are still lacking.

In low-dimensional magnets, the spatial arrangement of magnetic atoms is often deceptive, since the magnetic couplings do not show a clear correlation with distances between these atoms. In contrast, symmetries and overlaps of individual atomic orbitals play a crucial role.[19–22] In the following, we provide an instructive example that demonstrates the relevance of these characteristics for the microscopic magnetic model. We show that the β modification of $Cu_2V_2O_7$, previously considered as a spin-chain or a spin-dimer compound,[23–25] is the best available realization of the spin-$\frac{1}{2}$ Heisenberg model on the honeycomb lattice. To arrive at this unexpected conclusion, we first examine the crystal structure and analyze available experimental results (Sec. II). Based on qualitative arguments, we rule out the previously assumed spin-chain scenario and further evaluate the relevant exchange couplings along with the appropriate spin model in a microscopic study (Sec. IV). In Sec. V, we perform simulations for the proposed spin model and confirm our results by a direct comparison to the experimental data. We conclude our work with Sec. VI that reviews the unusual implementation of the honeycomb spin lattice in β-$Cu_2V_2O_7$ and provides an outlook for future experiments.

II. CRYSTAL STRUCTURE AND MAGNETIC PROPERTIES

Experimental studies of β-$Cu_2V_2O_7$ reveal low-dimensional magnetic behavior with predominantly antifer-

 ©2010 The American Physical Society

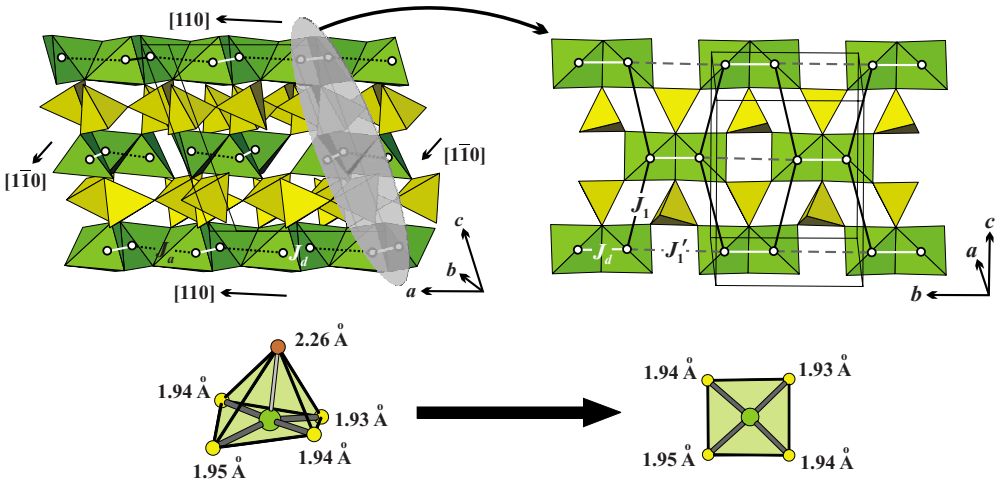

FIG. 1. (Color online) Crystal structure of β-$Cu_2V_2O_7$ with copper and vanadium polyhedra colored in green (dark) and yellow (light), respectively. The left panel shows chains of edge-sharing CuO_5 pyramids running along [110] and [1$\bar{1}$0]. The right panel presents a single layer of CuO_4 plaquettes in the *bc* plane, also indicated by a shaded area in the left panel. Individual exchange couplings are labeled by dark solid (J_1), dashed (J_1'), light solid (J_d), and dotted (J_a) lines. The bottom part of the figure presents different representations of the Cu local environment: the CuO_5 pyramid (left) and the CuO_4 distorted plaquette (right). The spin lattice is shown in Fig. 6.

romagnetic (AFM) couplings (the Curie-Weiss temperature $\theta \simeq 82$ K).[24] The temperature dependence of the magnetic susceptibility has a broad maximum at 50 K, followed by the magnetic ordering transition at $T_N = 26$ K.[24] The compound is controversially ascribed to different spin models. Two experimental studies applied the uniform-chain description,[23,24] whereas Touaiher *et al.*[26] claimed a better susceptibility fit presuming the spin-dimer model. Further on, band-structure calculations suggested two alternating couplings along the spin chains.[25] Surprisingly, all the three proposals are quite different from the actual spin lattice. Below we demonstrate that empirical considerations in the experimental studies[23,24,26] do not take account of the peculiar electronic structure of β-$Cu_2V_2O_7$ while the computational study[25] failed to resolve all the relevant exchange interactions in the compound.

The crystal structure of β-$Cu_2V_2O_7$ is of the framework type. Cu atoms have fivefold square-pyramidal coordination which is better described as "4+1" (see the bottom panel of Fig. 1). Four oxygen atoms in the *bc* plane reveal shorter bonds to Cu (1.93–1.95 Å) (Ref. 27) and form a CuO_4 plaquette, typical for Cu^{+2}. The fifth oxygen atom shows a longer bond of 2.26 Å which is roughly perpendicular to the plaquette along the *a* axis. The distance between the apical oxygen atom and the mean plane of the CuO_4 plaquette is about 2.2 Å. Considering the Cu polyhedron as a pyramid, one finds edge-sharing connections to one neighbor along the *b* direction and to one neighbor along *a*, thus chains along [110] and [1$\bar{1}$0] are formed (upper left panel of Fig. 1). As the representation of the Cu environment is reduced to the plaquette (right part of Fig. 1), the connection along *a* is broken, and we find Cu_2O_6 dimers of edge-sharing plaquettes (upper right panel of Fig. 1). Single VO_4 tetrahedra link such dimers within the *bc* planes while the pyrovanadate $[V_2O_7]$ groups join the resulting layers into a framework.

Overall, the structure looks quite complex. A first guess on the possible magnetic interactions is to consider shortest Cu-Cu distances for the edge-sharing pyramids: 2.95 Å along *b* (the interaction J_d within the structural dimers) and 3.26 Å along *a* (the interaction J_a). The resulting bonds form an alternating J_a–J_d chain proposed in Ref. 25 (left panel of Fig. 1). Other models assume the dimer limit ($J_d \gg J_a$) (Ref. 26) or the uniform chain limit $J_d \simeq J_a$.[23,24] However, neither of these assumptions is correct due to the inappropriate choice of the leading couplings. The formation of a CuO_4 plaquette is a clear signature of the magnetic (half-filled) orbital of $d_{x^2-y^2}$ symmetry, typical for Cu^{+2} with its $3d^9$ electronic configuration. In β-$Cu_2V_2O_7$, the plaquettes are slightly distorted. However, such a distortion has little effect on the crystal-field splitting, as confirmed by band-structure calculations for β-$Cu_2V_2O_7$ (Sec. IV) and for other Cu^{+2} compounds.[22]

The magnetic orbital lies in the plane of the plaquette (*bc*) and does not overlap with the orbitals of the fifth, apical oxygen atom. This feature, further confirmed by band-structure calculations (Fig. 4), allows us to reduce the local environment of Cu to the CuO_4 plaquette, despite the presence of five Cu-O bonds in the crystal structure. The position of the magnetic orbital makes the coupling J_a negligible (see Ref. 28 for a similar example). The coupling J_d is still allowed for the $d_{x^2-y^2}$ orbital. However, this coupling corresponds to the Cu-O-Cu angle of 98.7° implying sizable AFM and ferromagnetic (FM) contributions that might cancel each other.[22] These semiempirical arguments are readily confirmed by our band-structure calculations (Sec. IV) and hint at relevant exchange couplings beyond the structural nearest neighbors.

After resorting to the CuO_4 plaquette description and considering the *bc* plane as a potential magnetic layer, we find a remarkable similarity to the $(VO)_2P_2O_7$ structure (upper panel of Fig. 1).[29] This similarity is not surprising due to the similar (effective) $A_2B_2X_7$ composition. In fact, β-$Cu_2V_2O_7$ and $(VO)_2P_2O_7$ also share similar interpretation problems because the symmetry of the magnetic orbital determines possible superexchange pathways and renders some of the

short V-V contacts magnetically "inactive." Thus, the early misleading conjecture[30] on the spin ladder physics in $(VO)_2P_2O_7$ was based on the incorrect assumption of the strong coupling via the V-O-V superexchange pathway, although this pathway lacks any magnetically active orbital (similar to J_a in β-$Cu_2V_2O_7$).[19] As one further employs the structural analogy between β-$Cu_2V_2O_7$ and $(VO)_2P_2O_7$, a strong AFM coupling J_1' and alternating $J_1'-J_d$ chains along the b direction could be expected (right panel of Fig. 1). Yet, certain features of the electronic structure are different, thus even the $J_1'-J_d$ scenario of $(VO)_2P_2O_7$ has to be modified. Below, we show that the rearrangement of the cations (vanadium occupies the tetrahedral position and becomes nonmagnetic, copper takes the vanadium position) strongly affects the electronic structure. As a result, the spin system becomes 2D and attains the honeycomb-lattice geometry.

III. METHODS

To obtain a reliable microscopic model of β-$Cu_2V_2O_7$, we perform extensive density-functional theory (DFT) band-structure calculations using the full-potential local-orbital scheme (FPLO9.00–33).[31] We apply the local-density approximation (LDA) with the exchange-correlation potential by Perdew and Wang.[32] To cross-check the results, we used three alternative computational schemes: (i) the generalized gradient approximation (GGA) (Ref. 33) for the exchange-correlation potential within FPLO; (ii) the Vienna *ab initio* simulation package (VASP) (Ref. 34) with the basis set of projected augmented waves;[35] (iii) the tight-binding scheme for linearized muffin-tin orbitals in atomic spheres approximation (TB-LMTO-ASA),[36] where a different procedure for the evaluation of the exchange couplings is implemented. The typical k mesh included 1098 points in the symmetry-irreducible part of the first Brillouin zone for the crystallographic unit cell (LDA calculation) and 288 points for the supercell (DFT+U calculations). We use the structural data[27] from Ref. 37 as well as the data from Ref. 38. The results for the two structures match very well with the largest deviation below 10% for one of the leading exchange couplings.

The bare LDA approach does not provide a realistic description for the electronic ground state of transition-metal compounds due to the underestimate of strong correlation effects in the $3d$ shell. Nevertheless, LDA results can be taken as a reliable input for the modeling. Following this idea, we extract the relevant LDA valence bands and fit them with a one-orbital tight-binding (TB) model using Wannier functions (WFs) centered on Cu sites.[39] The application of the WF technique leads to the unambiguous evaluation of hopping parameters t_i and provides a clear picture of the magnetic orbitals. Further on, we introduce the hopping parameters into a Hubbard model with the effective on-site Coulomb repulsion $U_{\rm eff}$. The Hubbard model is then reduced to the Heisenberg model to describe the low-lying excitations. This reduction is justified by the half-filling and by the strongly correlated ($t_i \ll U_{\rm eff}$) regime. The parameters of the Heisenberg model are expressed as $4t_i^2/U_{\rm eff}$ and describe the AFM part $J_i^{\rm AFM}$ of the exchange. The parameter $U_{\rm eff}$ is fixed at 4.5 eV, according to previous studies.[20,22,40]

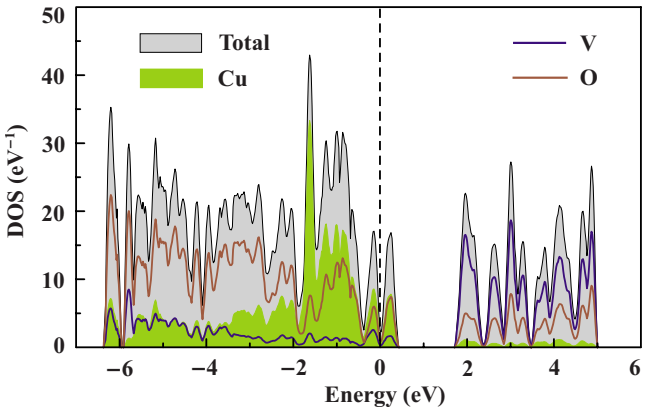

FIG. 2. (Color online) Total and atomic-resolved LDA DOS for β-$Cu_2V_2O_7$. The Fermi level is at zero energy.

The second approach to the evaluation of the exchange couplings includes a mean-field treatment of correlation effects via the local spin-density approximation (LSDA)+U (or the related GGA+U) method. Two options are possible: (i) total energies for a set of collinear spin configurations are mapped onto a classical Heisenberg model (supercell approach); (ii) the exchange integrals are treated as second derivatives of the energy with respect to the rotation of the magnetic moments; such derivatives are calculated via matrix elements of the Green's function [Lichtenstein exchange integral procedure (LEIP)].[41] The former approach is realized in FPLO and VASP while the latter is implemented in the TB-LMTO-ASA code. The on-site exchange parameter of the LSDA+U method was fixed at $J_{3d}=1$ eV. The choice of the Coulomb repulsion parameter U_{3d} is further discussed in Sec. IV B.

The DFT-based microscopic model was challenged by the experimental magnetic susceptibility data and the magnetic ordering temperature, taken from Ref. 24. The respective quantities as well as the high-field magnetization curves, static structure factors, and spin correlations were computed via quantum Monte Carlo (QMC) simulations with the loop algorithm[42] or the directed loop algorithim in the stochastic series expansion representation,[43] as implemented in the ALPS simulation package.[44] The simulations are done for finite lattices with periodic boundary conditions. The typical lattice size was 16×16 (512 sites) for the 2D model (magnetic susceptibility, high-field magnetization, spin correlations, ordered moment) and up to $16\times16\times12$ (6144 sites) for the three-dimensional (3D) model (magnetic ordering temperature). The results obtained on lattices of different size ensured the lack of appreciable finite-size effects. To determine the ordered moment, we calculated static structure factors at a constant temperature $T/\bar{J}_1=0.01$ and performed finite-size scaling, following Ref. 5.

IV. EVALUATION OF THE EXCHANGE COUPLINGS

A. LDA-based model

The main features of the LDA density of states (DOS, Fig. 2) are typical for Cu^{+2} compounds.[22,40,45] Essentially, the va-

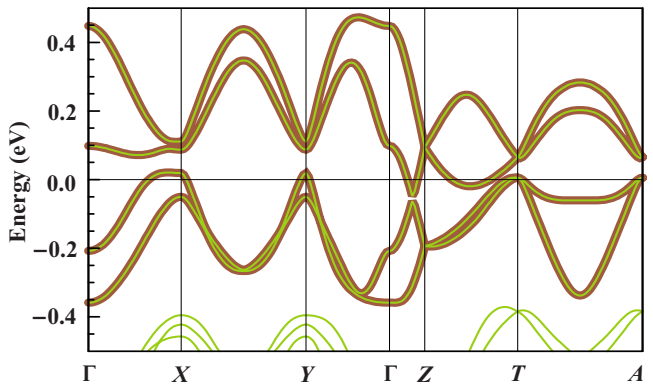

FIG. 3. (Color online) LDA bands at the Fermi level (thin light lines) and the fit of the tight-binding model (thick dark lines). The notation of the k points is as follows: $\Gamma(0,0,0)$, $X(0.5,0,0)$, $Y(0,0.5,0)$, $Z(0,0,0.5)$, $T(0.5,0,0.5)$, and $A(0,0.5,0.5)$, and the coordinates are given along k_x, k_y, and k_z in units of the respective reciprocal lattice parameters.

lence bands are a mixture of Cu and O states with a small contribution of vanadium. These bands lie between −6.5 and 0.5 eV and account for the bonding between Cu and the five neighboring oxygen atoms in the CuO_5 pyramid. The bands with the predominant vanadium contribution are found above 1.5 eV in agreement with the oxidation state of +5 for V atoms. The nearly isolated band complex at the Fermi level (Fig. 3) is mostly formed by the magnetic Cu $d_{x^2-y^2}$ orbital and the hybridizing $2p_\sigma$ orbitals of the four oxygen atoms comprising the CuO_4 plaquette. The magnetic orbital lies in the plane of the plaquette and determines possible superexchange pathways (see Sec. II). The energy spectrum is metallic due to the well-known shortcoming of LDA for strongly correlated systems. LSDA+U reproduces the insulating spectrum in agreement with the experimental identification of β-$Cu_2V_2O_7$ as a magnetic insulator.[23,24,46]

The TB fit of the Cu $d_{x^2-y^2}$ bands (Fig. 3) yields three leading AFM interactions in the bc plane: within the dimers (J_d), between the dimers along the b direction (J_1'), and between the dimers along [210] or [$\bar{2}$10] (J_1), see Table I. The nearest-neighbor interaction along a (J_a) is one of the leading magnetic couplings between the bc planes but it is much weaker than the next-nearest-neighbor in-plane couplings J_1 and J_1'. This supports our empirical, qualitative consider-

TABLE I. Cu-Cu distances (in Å), leading hopping parameters t_i (in meV) of the TB model, and the resulting AFM contributions to the exchange integrals J_i^{AFM} (in K). The exchange integrals are derived as $4t_i^2/U_{\mathrm{eff}}$ with the effective on-site Coulomb repulsion U_{eff}=4.5 eV.

	Distance	t_i	J_i^{AFM}
J_d	2.95	148	227
J_a	3.26	36	13
J_1	5.18	97	96
J_1'	5.25	−84	73
$J_\perp$	7.32	35	13

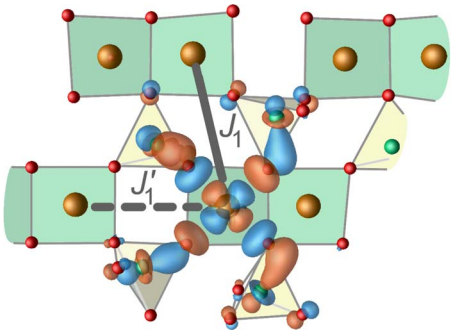

FIG. 4. (Color online) The Wannier function centered on the Cu site.

ations in Sec. II. Contrary to the spin-chain scenario, we propose a 2D model with leading exchange couplings in the bc plane. At first glance, the model approach would support the spin-dimer interpretation of Ref. 26 with the largest coupling J_d. However, the nearly 90° superexchange regime of J_d implies a large FM contribution that strongly modifies the TB scenario (see Sec. IV B).[47]

The couplings between the bc planes are below 15 K. In addition to the nearest-neighbor interaction J_a, we find the long-range couplings $J_\perp$ with similar energy. Despite the short Cu-Cu distance, J_a is small, since the magnetic orbital of Cu does not overlap with the orbitals of the apical oxygen atom and makes the Cu-O-Cu superexchange impossible. The couplings $J_\perp$ run via the V_2O_7 groups along (approximately) [111] and [1$\bar{1}$1] directions. Further hoppings in the TB model are below 25 meV, i.e., the respective J^{AFM}'s do not exceed 5–7 K and can be neglected within the minimum microscopic model.

The calculated WFs (Fig. 4) give a visual representation of the orbitals contributing to the superexchange. Each WF includes the Cu $d_{x^2-y^2}$ orbital and the p_σ oxygen orbitals along with the smaller contribution of vanadium orbitals. Since all the orbitals lie in the bc plane, the interplane couplings are relatively weak. Regarding the in-plane couplings, we note that oxygen contributions to WFs on the neighboring Cu sites show a nearly 90° arrangement for J_d. A similar arrangement is found for vanadium contributions with respect to J_1 and J_1'. This causes a FM contribution to the exchange due to the Hund's coupling on the ligand site.

Mazurenko *et al.*[47] developed a model for the ideal 90° superexchange geometry and calculated the FM part of the exchange: $J^{\mathrm{FM}}=-2\beta^4 J_H N_l$, where β is the ligand contribution to the WF, J_H is Hund's coupling on the ligand site, and N_l is the number of ligands where the WFs overlap (see also Ref. 21). In our case, $\beta_{\mathrm{O}}^2=0.10-0.12$, $\beta_{\mathrm{V}}^2\simeq 0.03$, and $N_l=2$. Assuming $J_H=1.5$ eV,[21,47] we find $J_d^{\mathrm{FM}}\simeq -850$ K and $J_1^{\mathrm{FM}}\simeq J_1'^{\mathrm{FM}}\simeq -60$ K. These values are rather overestimated (compare Tables I and II: $J_d^{\mathrm{FM}}\simeq -220$ K, $J_1^{\mathrm{FM}}\simeq -10$ K, and $J_1'^{\mathrm{FM}}\simeq -15$ K), yet they identify a sizable FM contribution to J_d along with order of magnitude smaller FM contributions to J_1 and J_1'. The overestimate is likely caused by the complex geometry of the system: the Cu-ligand distances are inequivalent, whereas the angles exceed 90° (e.g., the Cu-O-Cu angle for J_d is 98.7°), thus significantly reducing the Hund's coupling.

TABLE II. Exchange couplings calculated within LSDA+U. The columns list individual exchange integrals (in K), the Coulomb repulsion parameter U_{3d} of LSDA+U (in eV), the band-structure code, and the double-counting correction. The solutions consistent with the experiment are marked with the bold typeface.

J_d	J_a	J_1	J_1'	$J_\perp$	U_{3d}	Code	DCC
5	**−3**	**87**	**61**	**17**	**6**	**FPLO**	**AMF**
198	−9	100	121	37	6	FPLO	FLL
228	−10	108	125	38	7	VASP	FLL
232	0	83	50	14	9.5	LMTO	FLL
17	−3	**48**	**60**	**18**	**10**	**FPLO**	**FLL**

B. DFT+U

To evaluate full exchange integrals via DFT+U calculations, we consider the relevant in-plane couplings J_d, J_1, and J_1', as well as the two interplane couplings J_a and $J_\perp$. The results are collected in Fig. 5 and Table II. Most of the couplings are weakly dependent on the computational procedure but the estimate of J_d is highly sensitive to the U_d value and to details of the DFT+U method. The investigation of the respective methodological problems constitutes the main part of this section.

We start with the FPLO results shown in Fig. 5. Different exchange-correlation potentials (LSDA+U vs GGA+U, upper panel) have little effect on the exchange couplings. In contrast, the double-counting correction (DCC) scheme of DFT+U has a stronger effect on J's and especially influences J_d (bottom panel of the figure). The DFT+U method adds an explicit mean-field energy term to account for the Coulomb repulsion in the correlated shell. Then, a DCC is required. The DCC term subtracts a part of the repulsion energy that is already contained in LSDA (GGA). Several DCC schemes are available but their differences remain weakly explored.[48,49] In the FPLO code, two DCC schemes are implemented: around mean field (AMF)[50] and fully localized limit (FLL).[51]

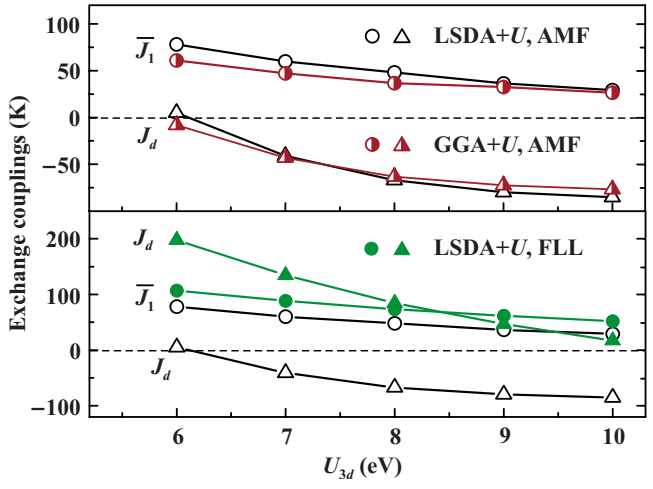

FIG. 5. (Color online) Exchange couplings $\bar{J}_1=(2J_1+J_1')/3$ (circles) and J_d (triangles) calculated with FPLO at different values of U_{3d}, the Coulomb repulsion parameter of DFT+U. The upper panel compares LSDA+U and GGA+U for the AMF double-counting correction scheme while the bottom panel compares two double-counting corrections for the LSDA+U functional (see text).

Band-structure calculations for a family of copper oxides have rather firmly established the proper U_{3d} value of 6–7 eV to reproduce the experimental exchange couplings within AMF.[20,40,45,52] Indeed, $U_{3d}=6$ eV in AMF leads to a reasonable scenario (first row of Table II). The interactions J_1, J_1', and $J_\perp$ are nearly unchanged compared to the TB estimates in Table I. This implies weak FM contributions in agreement with the long-range nature of these couplings. In contrast, the nearest-neighbor coupling J_d is reduced almost down to zero due to the superexchange pathway via the 98.7° bond angle. The other nearest-neighbor coupling J_a also has a FM contribution and becomes weakly FM. Since $|J_a|\leq 5$ K, this interaction can even be omitted in a minimum microscopic model. As the U_{3d} value is increased above 6 eV, the interactions J_1 and J_1' are slightly reduced, while J_d becomes FM.

Switching to FLL, we find a different scenario (Table II and the bottom part of Fig. 5). The couplings J_1 and J_1' are close to the AMF estimates. However, the short-range coupling J_d is about 200 K at $U_{3d}=6$ eV. As U_{3d} is increased to 10 eV, J_d becomes relatively smaller, resembling the AMF result at $U_{3d}=6$ eV. Overall, we can reliably estimate J_1, $J_1'=50-100$ K, while J_d can be either: (i) weak AFM (AMF, $U_{3d}=6$ eV or FLL, $U_{3d}=10$ eV); (ii) strong AFM (FLL, $U_{3d}=6$ eV); and (iii) strong FM (AMF, $U_{3d}\geq 8$ eV). In Sec. V, we carefully analyze the experimental data that unambiguously favor the first scenario. Unfortunately, this choice cannot be made on purely computational (i.e., *ab initio*) grounds. The DFT+U calculations are typically compared to the experimental band gap and to the ordered magnetic moments (sublattice magnetization). The sublattice magnetization of β-$Cu_2V_2O_7$ has not been reported and, anyway, should be subject to quantum effects (see Sec. V) that lie beyond DFT+U and preclude the reliable comparison. The experimental estimate of the band gap [$E_g=1.8$ eV (Ref. 46)] is in good agreement to both AMF ($E_g=2.0$ eV) and FLL ($E_g=1.75$ eV) results at $U_{3d}=6$ eV. As U_{3d} is increased to 10 eV, the band gap is somewhat overestimated ($E_g=2.3$ eV in FLL). Thus, the computational arguments would rather prefer the "typical" U_{3d} of 6 eV to describe the correlated electronic system of β-$Cu_2V_2O_7$. Yet, neither AMF nor FLL can be chosen unambiguously at this point.

The DCC problem is not unique to the FPLO code, although in other codes it may be left out due to the lack of alternative DCC schemes implemented. In VASP, only the FLL and the related Dudarev's approach[53] to the DCC are

available. According to previous studies,[54,55] we select U_{3d} =7 eV and find a remarkable agreement with the FPLO FLL results at U_{3d}=6 eV (see Table II). The 1 eV difference in U_{3d} is a typical offset due to the different basis sets (the Coulomb repulsion potential is applied to the atomic 3*d* orbitals which are basis-dependent). Further on, we used the LMTO code and determined U_{3d} from the constrained LDA procedure.[56] The resulting U_{3d} of 9.5 eV is in agreement with previous reports[21,47,57] and also leads to the typical FLL result with the large J_d.[58] Overall, different band-structure codes converge to the same FLL solution for the exchange integrals. In this solution, J_d largely exceeds J_1 and J_1' and contradicts the experimental energy scale (see Sec. V). To get a realistic solution with small J_d, one should either switch to the AMF DCC or take a larger U_{3d} value of about 10 eV for FPLO (and even larger values for VASP and LMTO).

The problem of the DCC choice is not specific to β-$Cu_2V_2O_7$, although in this compound it is probably most evident. Recently, we have shown that the AMF and FLL flavors of LSDA+*U* lead to different results for several Cu^{+2} compounds.[21,45,59] Similar to β-$Cu_2V_2O_7$, experimental data then favor the results at U_{3d}=6–7 eV for AMF and at U_{3d} =9–10 eV for FLL within FPLO.[45] This empirical recipe helps to adjust the U_{3d} value/the DCC scheme and to obtain realistic estimates of the exchange couplings. Still, a more general and comprehensive theoretical study of this computational effect is highly desirable.

The methodological part of the DFT+*U* study can be summarized as follows:

(i) the DCC scheme of DFT+*U* has influence on the exchange couplings and especially affects the short-range interactions;

(ii) The difference between the AMF and FLL flavors of DFT+*U* can be partly balanced by adjusting U_{3d}. However, the FLL results require unusually large U_{3d} values that look unjustified with respect to the typical estimates (e.g., from constrained LDA or from the comparison to the experimental band gap).

Switching back to the low-dimensional magnetism, we are able to construct a consistent microscopic picture, based on the TB analysis and the LSDA+*U* calculations. We establish a 2D spin model for β-$Cu_2V_2O_7$. The leading AFM interactions are J_1 and J_1' that act in the *bc* plane. The nonfrustrated interplane couplings $J_\perp$ amount to 10–15 K. The nearest-neighbor coupling J_d is somewhat ambiguous. However, the estimate of $J_d \simeq 200$ K clearly contradicts the experimental energy scale. A thorough analysis in Sec. V shows that J_d is essentially a weak coupling, well below J_1 and J_1'. The resulting J_1-J_1' spin system reveals three bonds per site and represents the anisotropic honeycomb lattice (Fig. 6). The coupling J_d between the structural nearest neighbors connects third neighbors on the spin lattice. Despite their complex structural arrangement, $J_\perp$ interactions can be considered as uniform interplane couplings.

V. SIMULATIONS AND COMPARISON TO THE EXPERIMENT

To challenge the proposed spin model by the experimental data and to investigate the properties of this model, we perform extensive QMC simulations. We start with the magnetic susceptibility[60] that was previously fitted with the expression for the uniform chain model.[24] This fit yield $J \simeq 79$ K and shows slight deviations from the experiment both at high temperatures and near the maximum (Fig. 7). The model of the isotropic honeycomb lattice with $\bar{J}_1$=66 K produces a significantly better fit which is in remarkable agreement with the experiment down to T_N (see the difference plot in Fig. 7).

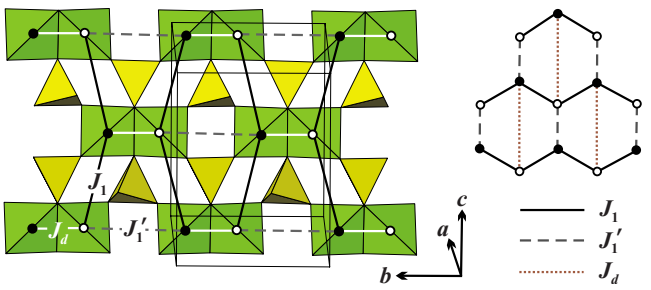

FIG. 6. (Color online) Crystal structure of β-$Cu_2V_2O_7$ and the sketch of the spin model with the leading couplings J_1 (solid lines) and J_1' (dashed lines). Dotted lines show J_d, the third-neighbor coupling on the honeycomb lattice. Open and shaded circles denote Cu atoms with opposite spins in the magnetically ordered ground state.

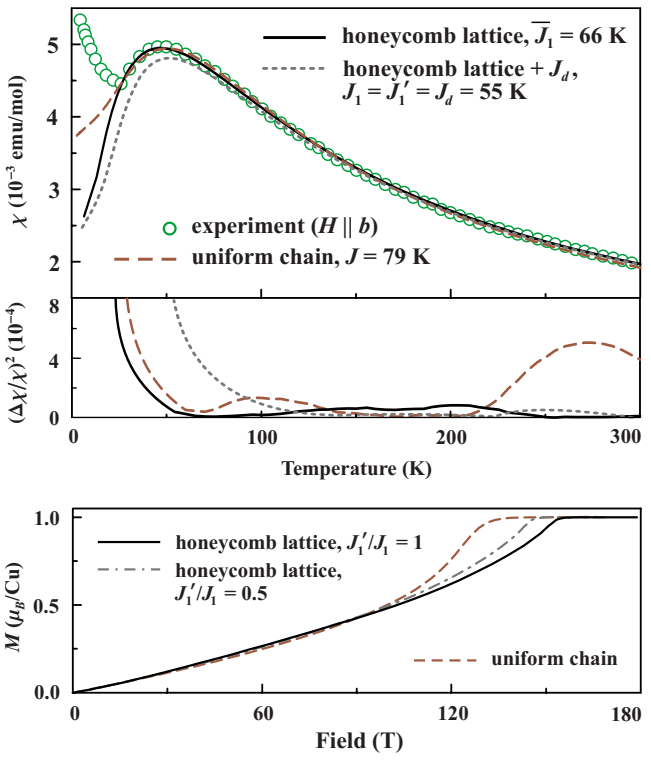

FIG. 7. (Color online) Upper panel: magnetic susceptibility of β-$Cu_2V_2O_7$ and the fits of the honeycomb-lattice (solid line), the uniform-chain (long-dashed line), and the honeycomb lattice with AFM J_d (short-dashed line) models. Experimental data are taken from Ref. 24. Difference curves are shown under the figure. Bottom panel: magnetization curves for the isotropic honeycomb lattice (solid line), anisotropic honeycomb lattice (dash-dotted line, J_1'/J_1 =0.5), and the uniform chain (dashed line) calculated at $T/\bar{J}_1$ =0.03.

Below T_N, the susceptibility is strongly dependent on the direction of the applied field and cannot be reproduced within the Heisenberg model that assumes isotropic exchange.

The low symmetry of the β-$Cu_2V_2O_7$ structure leads to a weakly anisotropic honeycomb lattice with inequivalent couplings J_1 and J_1'. However, this spatial anisotropy does not affect the magnetic susceptibility. We were able to fit the data down to T_N with $\bar{J}_1=(2J_1+J_1')/3=60-66$ K for $J_1'/J_1=0.5-1.3$ (the averaging includes two J_1 and one J_1' because there are two J_1 bonds and one J_1' bond per site). This situation resembles the anisotropic frustrated square lattice[61] where the moderate spatial anisotropy has little effect on the magnetic susceptibility. The fitted g value (1.9–2.2 depending on the field direction, in reasonable agreement with the powder-averaged $g\simeq 2.1$ from electron-spin-resonance measurements[23]) weakly depends on J_1'/J_1 and cannot be used to evaluate the degree of spatial anisotropy. Irrespective of the precise J_1'/J_1 ratio, the averaged coupling $\bar{J}_1$ is in excellent agreement with our computational estimates of 50–100 K for J_1 and J_1' (see Tables I and II).

To resolve the ambiguity regarding the size of J_d, we extended the model and introduced the third-neighbor coupling on the honeycomb lattice (right panel of Fig. 6). A small AFM J_d ($J_d/\bar{J}_1=0.2$) does not lead to any visible changes in the fit and slightly renormalizes $\bar{J}_1$. The effect of the moderate interplane coupling $J_\perp=0.2\bar{J}_1$ is similar to that of J_d. However, an AFM intradimer coupling on the order of $\bar{J}_1$ ($J_d=\bar{J}_1$) notably reduces the susceptibility maximum and leads to a poor fit of the data below 80 K (Fig. 7). A larger J_d of 150–200 K (as suggested by the FLL calculations, see Table II) clearly contradicts the experimental energy scale. Finally, the sizable FM coupling J_d would strongly frustrate the spin lattice and impede the long-range ordering. Our simulations for the unfrustrated lattice show excellent agreement with the experimental ordering temperature (see below), hence the scenario of strong FM J_d is unlikely. We conclude that the coupling J_d is weak while the leading couplings are J_1 and J_1' forming an anisotropic honeycomb lattice.

The magnetic ordering temperature T_N enables further comparison to the experimental data. To achieve the long-range ordering, we switch to a 3D model with an interplane coupling $J_\perp\simeq 13$ K$\simeq 0.2\bar{J}_1$ (cf. Table II). In a 3D model, the ordering transition is evidenced by a kink in the susceptibility curve or by a sharp increase in the staggered magnetization. To get a more accurate estimate, we calculate the Binder ratio $\langle m_s^4\rangle/\langle m_s^2\rangle^2$, where m_s is the staggered magnetization. The Binder ratio demonstrates a significant change upon the transition (Fig. 8). The intersection of the curves obtained for finite lattices of different size can be taken as a numerical estimate of T_N.[62] We find $T_N=0.41\bar{J}_1\simeq 27$ K in remarkable agreement with the experimentally observed $T_N=26$ K.[24] This comparison further supports our spin model. Similar to the magnetic susceptibility, the moderate spatial anisotropy ($J_1'/J_1=0.5-1.3$) has little effect on T_N (at $J_1'/J_1=0.5$, $T_N/\bar{J}_1=0.37$; at $J_1'/J_1=1.3$, $T_N/\bar{J}_1=0.40$).

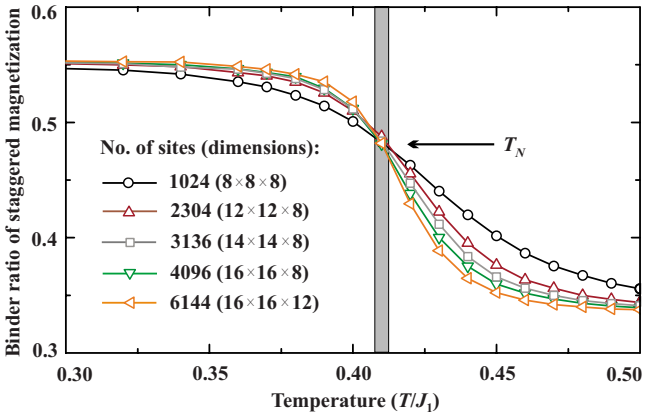

FIG. 8. (Color online) Binder ratio of the staggered magnetization $\langle m_s^4\rangle/\langle m_s^2\rangle^2$ for the isotropic honeycomb lattice with the interlayer coupling $J_\perp/\bar{J}_1=0.2$. Different symbols correspond to finite lattices of different size (note that the unit cell comprises two sites). The shaded bar shows the Néel temperature $T_N/\bar{J}_1\simeq 0.41$.

The temperature dependence of the magnetic susceptibility favors the honeycomb-lattice description of β-$Cu_2V_2O_7$ and yields the averaged coupling $\bar{J}_1$. However, the magnitude of the spatial anisotropy J_1'/J_1 cannot be precisely estimated. For the anisotropic frustrated square lattice compounds, high-field magnetization measurements are the most suitable tool to evaluate the spatial anisotropy.[63] Therefore, we also simulated magnetization curves of β-$Cu_2V_2O_7$ (see the lower panel of Fig. 7). The saturation field is slightly reduced for $J_1'/J_1<1$ due to the decrease in $\bar{J}_1$. The uniform-chain scenario would lead to an even lower saturation field of 130 T, compared to 145–155 T for the honeycomb lattice. However, the easily accessible field region up to 60 T shows negligible differences between the simulated curves. We conclude that high-field magnetization measurements could be a helpful tool to study the system, though only once the region around the saturation field (130–155 T) is reached.

Since the honeycomb spin lattice in β-$Cu_2V_2O_7$ may be slightly anisotropic ($0.5\leq J_1'/J_1\leq 1.3$), we study the influence of this spatial anisotropy on the ground state. The isotropic ($J_1'/J_1=1$) lattice leads to the largest m of about 0.54 μ_B. The spatial anisotropy reduces the dimensionality of the system and, consequently, reduces m down to 0.47 μ_B for $J_1'/J_1=0.5$ and down to 0.44 μ_B for $J_1'/J_1=1.5$ (Fig. 9). Although the magnitude of the effect is 15–20 %, it may be hard to resolve experimentally due to the low absolute values of m and the high uncertainty of experimental estimates (typically, above 10%). We also note that the interlayer coupling will rather increase the dimensionality leading to a slight increase in the m value.

Spin correlations are a sensitive probe for the ground-state properties. Therefore, we calculate the expectation values $\langle S_0S_R\rangle$ for $R=1-7$ running along the J_1 chains and in the perpendicular direction (see the inset of Fig. 10). For the isotropic (ideal) honeycomb lattice, both paths yield the same correlations (Fig. 10, bold lines). The spatial anisotropy $J_1'/J_1\neq 1$ slightly affects the correlations: for $J_1'/J_1<1$, the enhancement of spin correlations along the J_1 chains is ac-

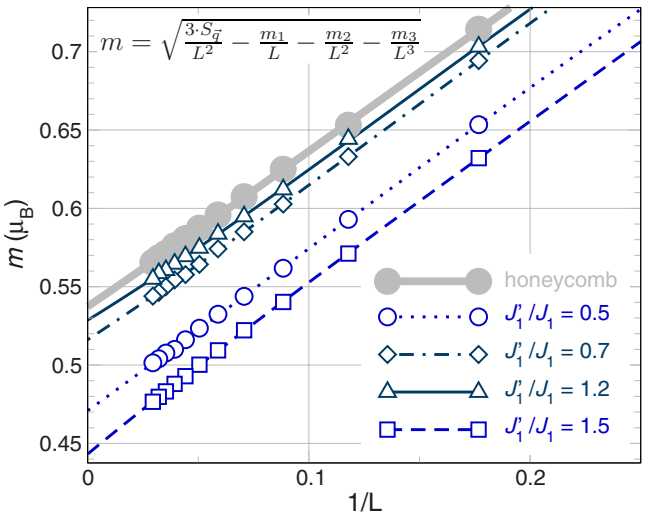

FIG. 9. (Color online) Finite-size scaling for the ordered moment (sublattice magnetization, m) of the anisotropic honeycomb lattice model. L is the period of the finite lattice (cluster size) and $S_{\vec{q}}$ is the static structure factor at the propagation vector $\vec{\mathbf{q}}$.

companied by the weakening in the perpendicular direction. In contrast, the correlations between the chains become stronger for $J_1'/J_1 > 1$. Although such a behavior is not surprising and follows the simple physical picture of strong and weak bonds, the similarity of the curves corresponding to different J_1'/J_1 is remarkable. Figure 10 evidences that the spin correlations strongly resemble the behavior of the isotropic honeycomb lattice, even for a sizable spatial anisotropy J_1'/J_1. This suggests that despite the spatial anisotropy, β-$Cu_2V_2O_7$ is a surprisingly good realization of the spin-$\frac{1}{2}$ Heisenberg model on the honeycomb lattice.

VI. DISCUSSION AND CONCLUSIONS

Based on a thorough microscopic study, we interpret the magnetic behavior of β-$Cu_2V_2O_7$ within the spatially anisotropic honeycomb model. Recent theoretical reports show that the properties of this model depend on the magnitude of the spatial anisotropy.[64] For strong dimer anisotropy ($J_1'/J_1 > 1.85$), a spin gap is opened, typical for a system of weakly coupled spin dimers. In contrast, a weak anisotropy leads to the honeycomb-lattice physics with the Néel AFM ordering. Our estimates of individual exchange couplings suggest $J_1'/J_1 = 0.5-1.3$ and place β-$Cu_2V_2O_7$ in the region of the Néel ordering, consistent with the experiment.[24] An AFM coupling J_d will further stabilize this ordering, while a FM J_d will induce magnetic frustration. Our estimate of $|J_d|/\bar{J}_1 \leq 0.2$ suggests that the effect of J_d should be relatively weak. Nevertheless, theoretical studies of the $J_1-J_1'-J_d$ model with the nonobvious *ferromagnetic* third-neighbor coupling J_d are desirable and could be relevant for related systems.

The magnetic structure of β-$Cu_2V_2O_7$ should bear further signatures of the underlying honeycomb spin lattice. The pronounced two-dimensionality and the low coordination number (three bonds per site) will lead to a strongly suppressed ordered moment of about 0.45–0.55 μ_B,[6] well below the classical value. A similar ordered moment is found in green dioptase with its peculiar 3D spin lattice that comprises three bonds per site only.[45] In β-$Cu_2V_2O_7$, the spin arrangement should feature antiparallel ordering along J_1 and J_1' that further leads to an antiparallel ordering within the structural dimers (see Fig. 6). The expected propagation vector is $\mathbf{k}=0$ (with respect to the atomic lattice) but the C centering of the atomic structure has to be broken. In contrast, the AFM ordering within the J_a-J_d chains does not violate the C centering. Thus, neutron-diffraction experiments are a feasible test for the proposed 2D model of β-$Cu_2V_2O_7$. Inelastic neutron scattering should be able to resolve individual couplings and to give a direct confirmation for the leading couplings J_1 and J_1'. Additionally, the

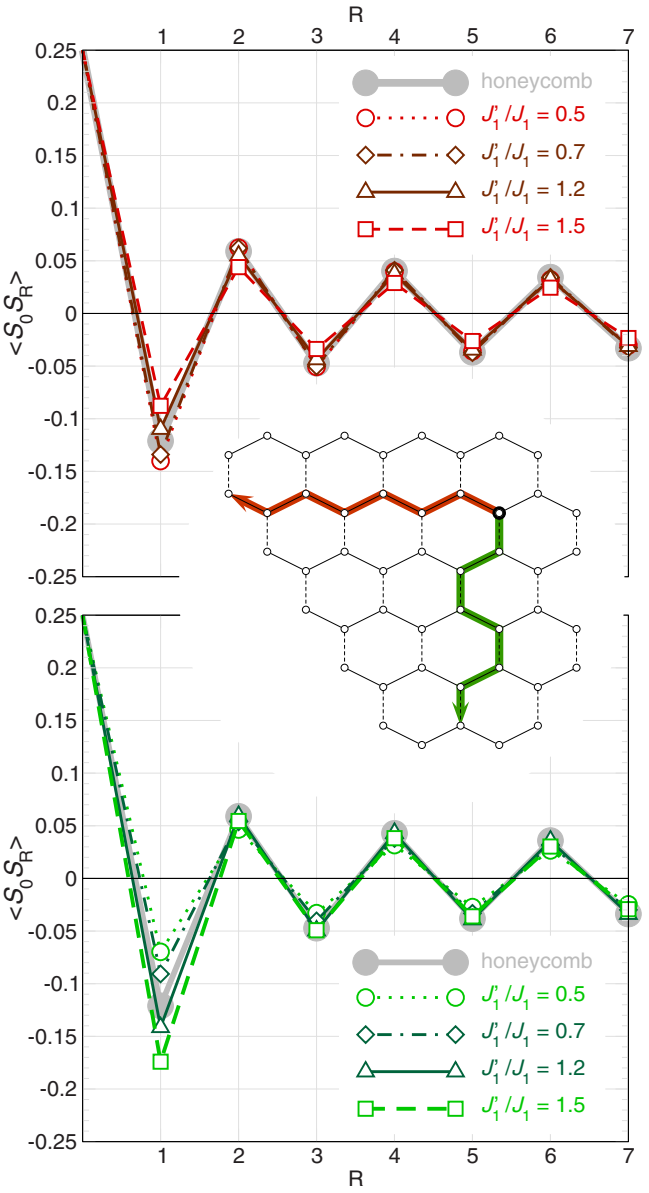

FIG. 10. (Color online) Spin correlations for different spatial anisotropies J_1'/J_1 compared to the isotropic honeycomb lattice (bold lines) along the J_1 chains (top) and in the perpendicular direction (bottom). The inset shows the respective paths, J_1 and J_1' are depicted by solid and dashed lines, respectively.

excitation spectrum of the spin-$\frac{1}{2}$ honeycomb lattice can be studied.

β-$Cu_2V_2O_7$ gives an instructive example of nontrivial magnetic interactions in transition-metal compounds. The symmetry of the magnetic orbital along with the Cu-O-Cu angle of 98.7° in the structural dimer disfavor sizable exchange couplings between the structural nearest neighbors. Then, the long-range couplings come into play. The situation largely resembles $VO(HPO_4)\cdot 0.5H_2O$ (Ref. 65) or $Cu_2(PO_3)_2CH_2$ (Ref. 22) where spin dimers do not coincide with the structural dimers. Another relevant example is $BiCu_2PO_6$ with its rungs of the spin ladder running *between* the structural ribbons.[54,59] Such intricate implementation of the long-range superexchange couplings is an abundant well of surprises, as in the present study. β-$Cu_2V_2O_7$ reveals a spin-$\frac{1}{2}$ honeycomb lattice, despite lacking any apparent structural features of the honeycomb geometry. We note that the isostructural $Cu_2P_2O_7$ and $Cu_2As_2O_7$ compounds could show similar features and deserve further investigation.

In summary, we have shown that β-$Cu_2V_2O_7$, previously considered as a spin-chain compound, should be consistently described as a honeycomb-lattice system. The leading couplings J_1 and J_1' run via the nonmagnetic VO_4 tetrahedra while the couplings between the structural nearest neighbors are weak. The averaged coupling $\bar{J}_1$ amounts to 60–66 K. The spatial anisotropy is relatively small and has little influence on the ordered moment as well as on spin correlations. The interlayer coupling $J_\perp \simeq 13$ K leads to the Néel antiferromagnetic ordering at $T_N = 25-30$ K. We propose that β-$Cu_2V_2O_7$ shows a relatively low sublattice magnetization of 0.45–0.55 μ_B, typical for the spin-$\frac{1}{2}$ honeycomb lattice. Further tests of our model should include high-field magnetization measurements, neutron diffraction, and inelastic neutron scattering. We conclude that β-$Cu_2V_2O_7$ is a noteworthy experimental realization of the spin-$\frac{1}{2}$ Heisenberg model on the honeycomb lattice. The convenient energy scale and the lack of disorder make it a promising system to challenge experiment and theory and to improve our understanding of low-dimensional magnets.

ACKNOWLEDGMENTS

We acknowledge Vladimir Mazurenko and Vladimir Anisimov for providing the TB-LMTO-ASA code with the LEIP option. We are also grateful to Johannes Richter, Alim Ormeci, and Juri Grin for careful reading of the manuscript and fruitful discussions. A.T. acknowledges the financial support from Alexander von Humboldt Foundation.

*altsirlin@gmail.com
†janson@cpfs.mpg.de
‡helge.rosner@cpfs.mpg.de

[1] L. Balents, Nature (London) **464**, 199 (2010).
[2] J. D. Reger, J. A. Riera, and A. P. Young, J. Phys.: Condens. Matter **1**, 1855 (1989).
[3] J. Oitmaa, C. J. Hamer, and Zheng Weihong, Phys. Rev. B **45**, 9834 (1992).
[4] J. Richter, J. Schulenburg, and A. Honecker, *Quantum Magnetism* (Springer, New York, 2004), Chap. 2, pp. 85–153.
[5] E. V. Castro, N. M. R. Peres, K. S. D. Beach, and A. W. Sandvik, Phys. Rev. B **73**, 054422 (2006).
[6] U. Löw, Condens. Matter Phys. **12**, 497 (2009).
[7] J. B. Fouet, P. Sindzingre, and C. Lhuillier, Eur. Phys. J. B **20**, 241 (2001).
[8] K. Takano, Phys. Rev. B **74**, 140402(R) (2006).
[9] A. Mulder, R. Ganesh, L. Capriotti, and A. Paramekanti, Phys. Rev. B **81**, 214419 (2010).
[10] A. Kitaev, Ann. Phys. **321**, 2 (2006).
[11] A. Willans, J. Chalker, and R. Moessner, Phys. Rev. Lett. **104**, 237203 (2010).
[12] N. Rogado, Q. Huang, J. W. Lynn, A. P. Ramirez, D. Huse, and R. J. Cava, Phys. Rev. B **65**, 144443 (2002).
[13] O. Smirnova, M. Azuma, N. Kumada, Y. Kusano, M. Matsuda, Y. Shimakawa, T. Takei, Y. Yonesaki, and N. Kinomura, J. Am. Chem. Soc. **131**, 8313 (2009).
[14] J. Chaloupka, G. Jackeli, and G. Khaliullin, Phys. Rev. Lett. **105**, 027204 (2010).
[15] Y. Miura, R. Hirai, Y. Kobayashi, and M. Sato, J. Phys. Soc. Jpn. **75**, 084707 (2006).
[16] Y. Miura, Y. Yasui, T. Moyoshi, M. Sato, and K. Kakurai, J. Phys. Soc. Jpn. **77**, 104709 (2008).
[17] A. Möller, U. Löw, T. Taetz, M. Kriener, G. André, F. Damay, O. Heyer, M. Braden, and J. A. Mydosh, Phys. Rev. B **78**, 024420 (2008).
[18] M. Yehia, E. Vavilova, A. Möller, T. Taetz, U. Löw, R. Klingeler, V. Kataev, and B. Büchner, Phys. Rev. B **81**, 060414(R) (2010).
[19] A. W. Garrett, S. E. Nagler, D. A. Tennant, B. C. Sales, and T. Barnes, Phys. Rev. Lett. **79**, 745 (1997).
[20] A. A. Tsirlin and H. Rosner, Phys. Rev. B **79**, 214416 (2009).
[21] A. A. Tsirlin and H. Rosner, Phys. Rev. B **81**, 024424 (2010).
[22] M. Schmitt, A. A. Gippius, K. S. Okhotnikov, W. Schnelle, K. Koch, O. Janson, W. Liu, Y.-H. Huang, Y. Skourski, F. Weickert, M. Baenitz, and H. Rosner, Phys. Rev. B **81**, 104416 (2010).
[23] J. Pommer, V. Kataev, K.-Y. Choi, P. Lemmens, A. Ionescu, Y. Pashkevich, A. Freimuth, and G. Güntherodt, Phys. Rev. B **67**, 214410 (2003).
[24] Z. He and Y. Ueda, Phys. Rev. B **77**, 052402 (2008).
[25] M. Yashima and R. O. Suzuki, Phys. Rev. B **79**, 125201 (2009).
[26] M. Touaiher, K. Rissouli, K. Benkhouja, M. Taibi, J. Aride, A. Boukhari, and B. Heulin, Mater. Chem. Phys. **85**, 41 (2004).
[27] We use the correct structural data with the O(4) atom at (0.2358, 0.7512, 0.3709). Due to a misprint, Ref. 37 reports a wrong position of this atom, as pointed out in Ref. 25. The wrong position is also clear from the comparison to the structure determination in Ref. 38.
[28] S.-L. Drechsler, J. Richter, A. A. Gippius, A. Vasiliev, A. A. Bush, A. S. Moskvin, J. Málek, Y. Prots, W. Schnelle, and H. Rosner, Europhys. Lett. **73**, 83 (2006).
[29] $(VO)_2P_2O_7$ has several polymorphic modifications with similar structures. β-$Cu_2V_2O_7$ is closest to the high-pressure form of $(VO)_2P_2O_7$.

[30] D. C. Johnston, J. W. Johnson, D. P. Goshorn, and A. J. Jacobson, Phys. Rev. B **35**, 219 (1987).
[31] K. Koepernik and H. Eschrig, Phys. Rev. B **59**, 1743 (1999).
[32] J. P. Perdew and Y. Wang, Phys. Rev. B **45**, 13244 (1992).
[33] J. P. Perdew, K. Burke, and M. Ernzerhof, Phys. Rev. Lett. **77**, 3865 (1996).
[34] G. Kresse and J. Furthmüller, Comput. Mater. Sci. **6**, 15 (1996); Phys. Rev. B **54**, 11169 (1996).
[35] P. E. Blöchl, Phys. Rev. B **50**, 17953 (1994); G. Kresse and D. Joubert, *ibid.* **59**, 1758 (1999).
[36] O. K. Andersen, Z. Pawlowska, and O. Jepsen, Phys. Rev. B **34**, 5253 (1986).
[37] D. Mercurio-Lavaud and B. Frit, C. R. Seances Acad. Sci., Ser. C **277**, 1101 (1973).
[38] J. M. Hughes and M. A. Brown, Neues Jahrb. Mineral., Monatsh., 41 (1989).
[39] H. Eschrig and K. Koepernik, Phys. Rev. B **80**, 104503 (2009).
[40] O. Janson, R. O. Kuzian, S.-L. Drechsler, and H. Rosner, Phys. Rev. B **76**, 115119 (2007).
[41] M. I. Katsnelson and A. I. Lichtenstein, Phys. Rev. B **61**, 8906 (2000).
[42] S. Todo and K. Kato, Phys. Rev. Lett. **87**, 047203 (2001).
[43] F. Alet, S. Wessel, and M. Troyer, Phys. Rev. E **71**, 036706 (2005), and references therein.
[44] A. Albuquerque, F. Alet, P. Corboz, P. Dayal, A. Feiguin, S. Fuchs, L. Gamper, E. Gull, S. Gürtler, A. Honecker, R. Igarashi, M. Körner, A. Kozhevnikov, A. Läuchli, S. R. Manmana, M. Matsumoto, I. P. McCulloch, F. Michel, R. M. Noack, G. Pawłowski, L. Pollet, T. Pruschke, U. Schollwöck, S. Todo, S. Trebst, M. Troyer, P. Werner, and S. Wessel, J. Magn. Magn. Mater. **310**, 1187 (2007).
[45] O. Janson, A. A. Tsirlin, M. Schmitt, and H. Rosner, Phys. Rev. B **82**, 014424 (2010).
[46] F. A. Benko and F. P. Koffyberg, Can. J. Phys. **70**, 99 (1992).
[47] V. V. Mazurenko, S. L. Skornyakov, A. V. Kozhevnikov, F. Mila, and V. I. Anisimov, Phys. Rev. B **75**, 224408 (2007).
[48] A. G. Petukhov, I. I. Mazin, L. Chioncel, and A. I. Lichtenstein, Phys. Rev. B **67**, 153106 (2003).
[49] E. R. Ylvisaker, W. E. Pickett, and K. Koepernik, Phys. Rev. B **79**, 035103 (2009).
[50] M. T. Czyżyk and G. A. Sawatzky, Phys. Rev. B **49**, 14211 (1994).
[51] V. I. Anisimov, I. V. Solovyev, M. A. Korotin, M. T. Czyżyk, and G. A. Sawatzky, Phys. Rev. B **48**, 16929 (1993).
[52] W. E. A. Lorenz, R. O. Kuzian, S.-L. Drechsler, W.-D. Stein, N. Wizent, G. Behr, J. Málek, U. Nitzsche, H. Rosner, A. Hiess, W. Schmidt, R. Klingeler, M. Loewenhaupt, and B. Büchner, Europhys. Lett. **88**, 37002 (2009).
[53] S. L. Dudarev, G. A. Botton, S. Y. Savrasov, C. J. Humphreys, and A. P. Sutton, Phys. Rev. B **57**, 1505 (1998).
[54] O. Mentré, E. Janod, P. Rabu, M. Hennion, F. Leclercq-Hugeux, J. Kang, C. Lee, M.-H. Whangbo, and S. Petit, Phys. Rev. B **80**, 180413(R) (2009).
[55] M. G. Banks, R. K. Kremer, C. Hoch, A. Simon, B. Ouladdiaf, J.-M. Broto, H. Rakoto, C. Lee, and M.-H. Whangbo, Phys. Rev. B **80**, 024404 (2009).
[56] O. Gunnarsson, O. K. Andersen, O. Jepsen, and J. Zaanen, Phys. Rev. B **39**, 1708 (1989).
[57] V. V. Mazurenko, S. L. Skornyakov, V. I. Anisimov, and F. Mila, Phys. Rev. B **78**, 195110 (2008).
[58] LEIP uses a unique spin configuration and may underestimate the FM superexchange because different spin polarizations of the ligands in the FM and AFM states are not considered (see Ref. 47 and Sec. IV A for details regarding the role of the Hund's coupling on the ligand site). Nevertheless, the LEIP results are in remarkable agreement with the exchange couplings from the supercell approach at properly adjusted U_{3d} (see Table II). This shows that the problem of the ligand polarization is a minor drawback of LEIP when applied to Cu^{+2} oxides.
[59] A. Tsirlin, I. Rousochatzakis, D. Kasinathan, O. Janson, R. Nath, F. Weickert, C. Geibel, A. Läuchli, and H. Rosner, arXiv:1008.1771 (to be published).
[60] Note that different studies report fairly different magnetic susceptibility data. For example, the susceptibility maximum is around 50 K in Refs. 23 and 24 while Ref. 26 reports the maximum at 15 K. In our analysis, we use the single-crystal data from Ref. 24 that look most accurate and reliable.
[61] A. A. Tsirlin and H. Rosner, Phys. Rev. B **79**, 214417 (2009).
[62] K. Binder, Rep. Prog. Phys. **60**, 487 (1997).
[63] A. A. Tsirlin, B. Schmidt, Y. Skourski, R. Nath, C. Geibel, and H. Rosner, Phys. Rev. B **80**, 132407 (2009).
[64] W. Li, S.-S. Gong, Y. Zhao, and G. Su, Phys. Rev. B **81**, 184427 (2010).
[65] D. A. Tennant, S. E. Nagler, A. W. Garrett, T. Barnes, and C. C. Torardi, Phys. Rev. Lett. **78**, 4998 (1997).